Comparative evaluation of two analytical methods for Helical Cone-Beam Tomography

Harald Schöndube*†, *Graduate Student Member, IEEE,* Karl Stierstorfer†,
Frank Dennerlein*, *Graduate Student Member, IEEE,* and Frédéric Noo*, *Member, IEEE*

***Abstract*—We present some extensions to the recently published "DBP-0" method which are important for making the algorithm more suitable for clinical routine. These extensions are (i) an incorporation of the slice thickness into the reconstruction process, (ii) a way of reconstructing a region of interest smaller than the FOV, (iii) the possibility to reconstruct from flying focal spot data and (iv) a frequency apodization scheme for influencing the resolution vs. noise level during reconstruction.**

We furthermore present an evaluation of the DBP-0 method against the approximate Weighted FBP (WFBP) algorithm in terms of resolution, noise and subjective appearance of reconstructed images.

I. Introduction

In recent years, several analytical approaches for image reconstruction from helical Cone-Beam CT (HCBT) data have been developed, see e.g. [1]–[4]. They can be divided into two groups: Mathematically exact methods and approximate methods. The second group has been preferred for use in commercial CT systems up to now. Their performance, however, decreases with increas in the cone angle, so that image quality can be significantly affected by cone beam artifacts for scanners with a large number of rows. This is not a problem for the group of exact methods, but, compared with approximate algorithms, the exact methods lack the ability of handling redundant data and are therefore less efficient in terms of dose usage and image noise suppression. Yet, with increasing cone angles in commercial CT scanners they might become the method of choice for routine image reconstruction.

We present a comparative evaluation of a mathematically algorithm against one from the group of approximate algorithms. For the exact algorithms we chose the "DBP-0" variant of the two-step Hilbert HT-DBP reconstruction which works on rebinned data [5]. From the second group we picked the Weighted FBP (WFBP) as one example of the approximate algorithms currently used in commercial CT scanners [4].

We first present a short outline of the DBP-0 method. Subsequently, some important extensions to the DBP-0 method will be studied. These extensions are aimed at making the algorithm more suitable for practical use in clinical scanners and include (i) incorporation of the slice thickness into the reconstruction process, (ii) a way of reconstructing a region of interest smaller than the FOV, (iii) the possibility to reconstruct from flying focal spot data and (iv) a frequency apodization scheme for influencing the resolution vs. noise level during reconstruction. For evaluation purposes we then compare resolution, noise and the subjective appearance of reconstructed images.

Manuscript received May 11, 2007. This work was supported in part by the U.S. National Institutes of Health (NIH) under grants R21 EB000568 and R01 EB000627, and in part by Siemens Medical Solutions. Its contents are solely the responsibility of the authors and do not necessarily represent the official views of the NIH.

*Department of Radiology, University of Utah, Salt Lake City, USA
†Siemens Medical Solutions, Forchheim, Germany
Harald Schöndube and Frédéric Noo can be contacted at {hschoend|noo}@ucair.med.utah.edu. Karl Stierstorfer can be contacted at karl.stierstorfer@siemens.com.

II. The DBP-0 reconstruction method

A. Data acquisition geometry

We use a standard data acquisition geometry with a curved detector consisting of $N_{rows} \times N_{cols}$ elements. The CT measurements of a volume $f(\underline{x})$ are given as $g(\lambda, \gamma, w)$ where γ is the fan angle and w the detector row index. The source position on the vertex path is given as

$$\underline{a}(\lambda) = [R_0 \cos(\lambda + \lambda_0),\ R_0 \sin(\lambda + \lambda_0),\ z_0 + h\lambda]\,, \qquad (1)$$

where λ is the rotation angle of the source in the interval $[0,\ \lambda_{\max}]$, R_0 is the helix radius and $2\pi h$ the helix pitch. The vertex path is adjusted by λ_0 and z_0 such that at $\lambda = 0$ the source is located at angle λ_0 in the plane $z = z_0$.

B. DBP-0

1) Backprojection geometry: DBP-0 is a variant of the differentiated backprojection [5] and thus does not result directly in a theoretically exact reconstruction of $f(\underline{x})$. Instead it yields its Hilbert transform $(\mathcal{H}f)(\underline{x})$ along certain lines within the volume. The exact location and direction of these lines can be chosen by adapting the backprojection algorithm accordingly. If the geometry is chosen correctly, an inverse Hilbert transform can then be performed along those lines followed by a final coordinate transform to Cartesian coordinates to obtain $\hat{f}(\underline{x})$, the theoretically exact reconstruction of $f(\underline{x})$.

DBP-0, which received this designation due to the lack of a backprojection weight, works on so called "π-lines", i.e. lines which intersect the vertex path twice with both intersections being located less than one helix turn from each other. Without loss of generality, DBP-0 can be restricted to working on π-lines having a positive slope. For backprojection, the π-lines are arranged into several surfaces such that the π-lines within one surface have their projections onto the (x, y)-plane parallel and equidistant to each other. One such surface is depicted in fig. 1.

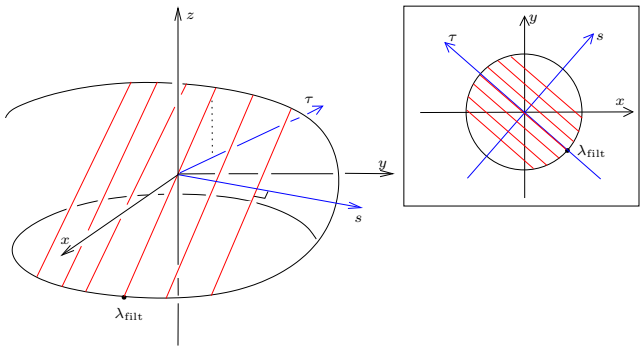

Fig. 1. Sketch of a surface of π-lines for a fixed λ_{filt}.

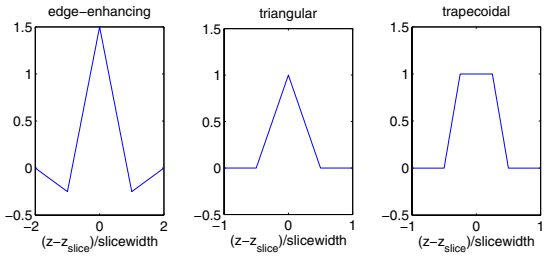

Fig. 2. The three different weighting schemes.

Each surface is indexed by a vertex position λ_{filt}, where $\underline{a}(\lambda_{\mathrm{filt}})$ denotes the starting point of a π-line which intersects with the z-axis. All π-lines on a given surface have their projections on the (x, y)-plane parallel to each other, and λ_{filt} defines the direction of these lines. Note, however, that by construction π-lines defined by the same λ_{filt} are *not* parallel in the z dimension. Yet, using proper interpolation can still be performed reconstruction using these surfaces.

For indexing onto each π-line surface a (s, τ)-grid is used which is obtained by rotating the x- and y-axes such that s denotes a signed distance of the projections of the π-lines onto the (x, y)-plane from the origin, and τ is a coordinate along those projections. The z-position of a point indexed by $(s, \tau, \lambda_{\mathrm{filt}})$ is given by

$$z = z_0 + h\left(\lambda_{\mathrm{filt}} + \frac{\pi}{2} + \frac{\tau\left(\pi/2 - \arcsin\left(s/R_0\right)\right)}{\sqrt{R_0^2 - s^2}}\right). \quad (2)$$

For a given desired volume (x, y, z), this equation also allows to determine the range of λ_{filt} over which backprojection should be carried out to cover the volume of interest.

2) The algorithm: The DBP-0 algorithm is based on a rebinning of the measured data to the pseudo-parallel "wedge" geometry according to

$$\vartheta(\lambda, \gamma) = \lambda + \frac{\pi}{2} - \gamma, \qquad s_{\mathrm{r}}(\lambda, \gamma) = R_0 \sin\gamma, \quad (3)$$

with w remaining untouched during rebinning. This approach offers the advantage of reducing the filtering to a single derivative $\partial/\partial s_{\mathrm{r}}$ and furthermore of neither requiring a backprojection distance weight nor a voxel-dependent backprojection range for voxels within any given surface of π-lines.

The backprojection formula after rebinning can be shown to be

$$(\mathcal{H}f)(\underline{x}) = -\frac{1}{2\pi}\int_{\vartheta_{\mathrm{filt}}}^{\vartheta_{\mathrm{filt}}+\pi} \frac{D \cdot \bar{g}_{\mathrm{rb}}(\vartheta, s_{\mathrm{r}}^*(\vartheta, \underline{x}), w^*(\vartheta, \underline{x}))}{\sqrt{D^2 + (w^*(\vartheta, \underline{x}))^2}}\,\mathrm{d}\vartheta \quad (4)$$

with

$$\bar{g}_{\mathrm{rb}}(\vartheta, s_{\mathrm{r}}, w) = \frac{\partial}{\partial s_{\mathrm{r}}} g_{\mathrm{rebin}}(\vartheta, s_{\mathrm{r}}, w), \quad (5)$$

$$s_{\mathrm{r}}^*(\vartheta, \underline{x}) = x\cos(\vartheta + \vartheta_0) + y\sin(\vartheta + \vartheta_0), \quad (6)$$

$$w^*(\vartheta, \underline{x}) = \frac{D\left(z - z_0 - h\left(\vartheta - \pi/2 + \arcsin\left(s_{\mathrm{r}}^*/R_0\right)\right)\right)}{y\cos(\vartheta + \vartheta_0) - x\sin(\vartheta + \vartheta_0) + \sqrt{R_0^2 - s_{\mathrm{r}}^{*2}}} \quad (7)$$

and $\vartheta_{\mathrm{filt}} = \lambda_{\mathrm{filt}} + \pi/2$ and $\vartheta_0 = \lambda_0 + \pi/2$.

The inverse Hilbert transform is performed the way it is described in [2] using the method first suggested by Soehngen [6] with a rectangular apodization window and a half-pixel shift of the output to avoid aliasing artifacts.

III. Some Extensions to the DBP-0 Method

We have developed some important extensions to the DBP-0 method which are aimed at making it more suitable for practical use in clinical scanners. These extensions are the incorporation of the desired slice thickness, the ability to limit computational effort when reconstructing a region of interest smaller than the FOV and the ability of using flying focal spot data.

A. A slice thickness method for DBP-0

The DBP-0 method does not yield a direct reconstruction of $f(\underline{x})$ in Cartesian coordinates but on the π-line surfaces described in section II-B1 instead. Thus, reformatting the data is necessary to finalize reconstruction. This reformatting is performed in two steps: In the first step, we bilinearly interpolate from the $(s, \tau, \lambda_{\mathrm{filt}})$ coordinates of the π-line surfaces to an intermediate $(x, y, \lambda_{\mathrm{filt}})$ coordinate system. In the second step these intermediate data (which are non-linearly spaced in the z direction) are reformatted to Cartesian coordinates.

A simple method for the second step is performing a linear interpolation between the two samples closest to the desired z location. A more sophisticated approach can be developed by adapting the slice thickness reformating method presented in [7] for the AMPR algorithm. This approach is based on building a weighted sum of all samples within a certain distance in z from the desired slice. Three different weighting schemes are applied: triangular, trapezoidal and edge-enhancing. A sketch of those three schemes is shown in fig. 2. The trapezoidal scheme is used for thick slices ($d_{\mathrm{slice}} > 2d_{\mathrm{row}}$, with d_{slice} denoting the desired slice width and d_{row} the width of the detector rows measured at the isocenter), the edge-enhancing scheme for very fine slices ($d_{\mathrm{slice}} < d_{\mathrm{row}}$). Sample reconstructions of a very thick slice and a thin slice are shown in fig. 3.

There is a computational cost cost associated with using this scheme, which arises from the need to use finer sampling of π-line surfaces during reconstruction, as it has to be made sure that the distance between two samples (and thus surfaces of π-lines) in z is smaller than or equal to the desired slicewidth everywhere within the desired volume. This means that more

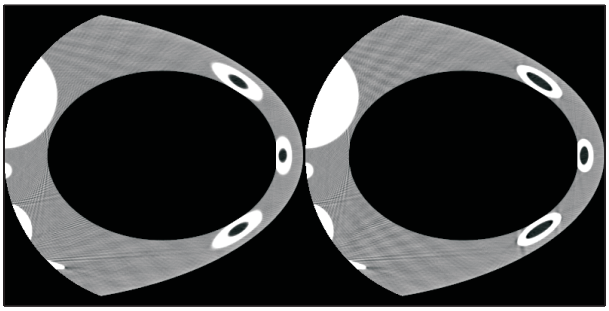

Fig. 3. Reconstruction results of the FORBILD thorax phantom using the slicewidth concept: (left) results with $d_{\mathrm{row}} = 0.75$ mm, $d_{\mathrm{slice}} = 5$ mm (trapezoidal weighting scheme); (right) results with $d_{\mathrm{slice}} = 0.5$ mm (edge-enhancing weighting scheme). Window: $-25 \ldots 25$ HU

surfaces of π-lines have to be reconstructed for the same desired range in z. We use a λ_{filt} spacing of

$$\Delta\lambda_{\mathrm{filt}} = \frac{d_{\mathrm{slice}}}{h \cdot \left(1 + \frac{\pi/2 + \arcsin R_{\mathrm{FOV}}/R_0}{\sqrt{1-(R_{\mathrm{FOV}}/R_0)^2}}\right)} \tag{8}$$

when using the slice thickness method compared to

$$\Delta\lambda_{\mathrm{filt}} = \frac{\Delta z}{h} \tag{9}$$

when using simple linear interpolation with Δz denoting the desired voxel size in z. For $R_{\mathrm{FOV}} = 25$ cm, $R_0 = 57$ cm, a helix pitch of 6.58 cm and $d_{\mathrm{slice}} = \Delta z$ this yields a factor of 3.25 between the two different methods.

B. ROI DBP-0

If the reconstruction range in the (x, y)-plane is confined to a circular, possibly off-center, region of interest (ROI) it is not economical to perform reconstruction over the whole FOV first and then cut out the ROI. We thus have developed some ways to limit computational effort when reconstructing a ROI using DBP-0.

An obvious and efficient way to reduce computational effort is to exclude those π-lines from the reconstruction process which do not intersect the ROI and thus don't contribute to the final volume. In other words, the backprojection range in s direction gets confined to those values which correspond to π-lines intersecting the ROI. It then varies whith λ_{filt} according to the location of the ROI. Confining the backprojection range in τ, in contrast, is generally not possible, as the inverse Hilbert transform has to be carried out over the function support; in practice this usually means over the full FOV. Thus the backprojection range in τ has to cover the whole FOV as in non-ROI reconstruction. A sketch of the set of π-lines needed for reconstruction of a certain ROI for two different values of λ_{filt} is shown in fig. 4.

A further approach of reducing computational load can be found in the fact that for reformatting the reconstructed data from the surfaces of π-lines to Cartesian coordinates a certain overhead in terms of number of slices needed for a desired volume in z is necessary. For reconstruction confined to a ROI smaller than the FOV it is usually possible to reduce this overhead by a certain amount. This amount varies greatly and

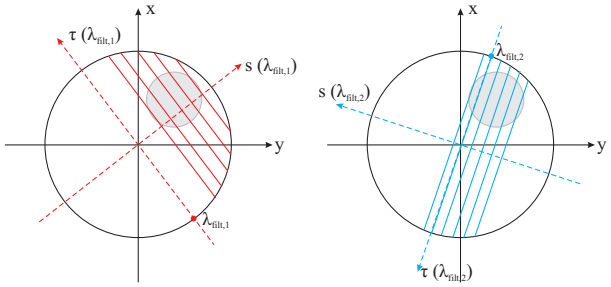

Fig. 4. Sets of π-lines for reconstruction of a certain ROI for two different values of λ_{filt}.

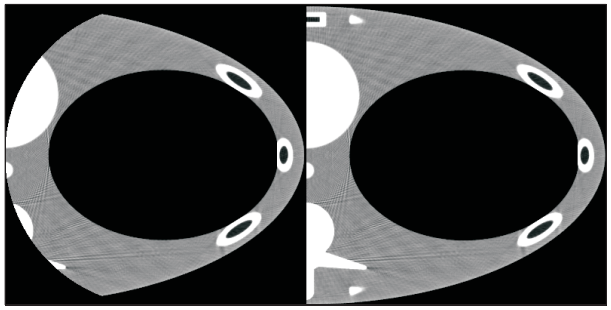

Fig. 5. Reconstruction result of the FORBILD thorax phantom for a ROI with $R_{\mathrm{ROI}} = 10$ cm centered on $(10, 0)$ (left). Corresponding part of a reconstruction performed over the full FOV (right). Window: $-25 \ldots 25$ HU

depends strongly from the exact location and size of the ROI, with a greater reduction being possible for ROIs which are small or located close to the center of the FOV.

Summarizing those adaptations, one should expect backprojection time being able to be reduced by at least the factor between the number of π-lines being needed per surface of π-lines for ROI reconstruction vs. reconstruction of the full FOV. This factor can be computed as $1 - R_{\mathrm{ROI}}/R_{\mathrm{FOV}}$, where R_{ROI} and R_{FOV} denote the radius of the ROI and the FOV, respectively. During our investigations we found that assumption to be true. In cases with a great reduction of the backprojection overhead an even greater reduction of backprojection time (up to five times that factor) was being observed. An example of a region reconstructed with the backprojection confined to a certain ROI vs. that same region reconstructed with the backprojection range covering the full FOV is shown in fig. 5.

C. DBP-0 and flying focal spot data

A desirable feature for clinical practice is the ability to process flying focal spot (FFS) data. Due to the rebinning nature of the DBP-0 algorithm, this is easily possible for a data acquired with a flying focal spot in lateral direction (i.e. in direction of the fan angle γ) as well as with an FFS in z direction. When doing so, processing of the FFS data takes place during rebinning with the backprojection itself remaining unchanged. After rebinning, a flying focal spot in z results in a doubling of the number of rebinned data rows, and a laterally flying focal spot results in a doubling of the number of channels within each rebinned data row.

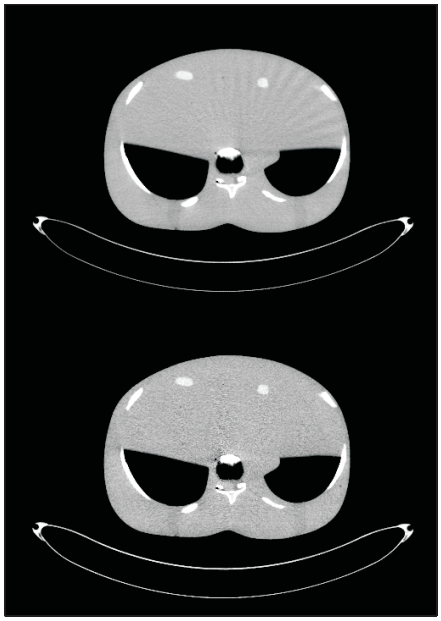

Fig. 6. Reconstructions of a thorax phantom from real data measured with an experimental 64-row scanner: no FFS (top), FFS in both z and γ directions (bottom). Window $-200 \ldots 200$ HU. Note that the FFS data was measured with $d_{\mathrm{row}} = 0.6$ mm whereas the non-FFS data was measured with $d_{\mathrm{row}} = 1.2$ mm and thus the noise level of the two reconstructions is not directly comparable due to a difference in z resolution.

Our experiments have shown that a notable reduction of windmill artifacts can be achieved when using data acquired with a FFS in z. Furthermore, resolution can be enhanced by using data with an FFS in γ. Sample reconstructions of a thorax phantom from real data measured with an experimental 64-row scanner with and without the flying focal spot are shown in fig. 6.

D. Frequency apodization during reconstruction

We have developed an easy way of setting a desired level of smoothness during the reconstruction process by filtering the data along the rows after rebinning and before performing the differentiated backprojection. By either enhancing or decreasing high frequency values we thus either enhance resolution and increase the noise level or lower both resolution and noise of the reconstruction result.

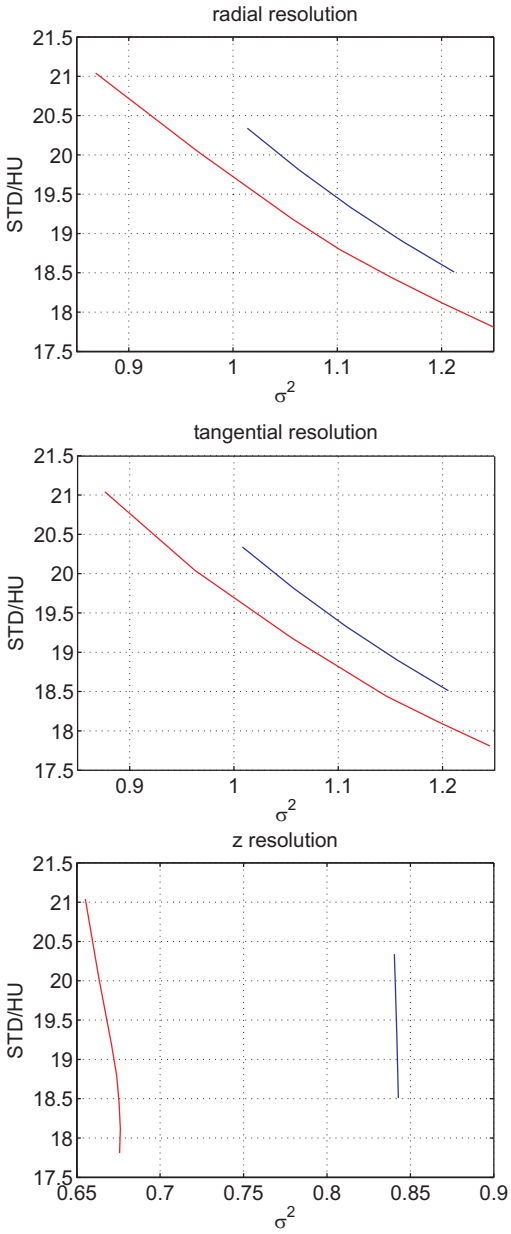

Fig. 7. Resolution vs. noise for DBP-0 (blue) and WFBP (red) in each radial, tangential and z direction. Note that we applied the "apodization" filter only along the rows of the rebinned data, so z resolution remains largely unaffected by this approach.

IV. Comparison of DBP-0 with WFBP

In the following we present a comparison of DBP-0 against WFBP, an approximate algorithm currently used in clinical CT scanners [4]. We have performed this comparison by means of evaluating resolution vs. noise and by visual inspection of the reconstruction results.

For measuring resolution we used a FORBILD thorax phantom into which we placed a spherical lesion of radius 0.5 cm at point $(0, -1 \text{ cm}, 0)$. Filtering the ground truth using a 3D Gaussian filter, we use the set of σ^2 values for which the difference between the reconstruction outcome and the filtered ground truth is minimal as resolution values in each radial, tangential and z direction. Noise values were obtained using the FORBILD thorax phantom without the sphere by averaging the standard deviation of seven noise realisations over a spherical region of radius 0.5 cm around the point $(0, -1 \text{ cm}, 0)$. We varied the desired resolution vs. noise level over several reconstructions of the same phantom using the technique described in section III-D and thus obtained a resolution/noise plot for each the radial, tangential and z resolution. Those plots are shown in fig. 7. Note that despite the data being plotted in three separate plots, one has only one degree of freedom in choosing those parameters. (One can e.g. choose a desired radial resolution, which delivers a corresponding noise level. From this noise level one then can obtain the corresponding tangential and z resolutions from their respective plots).

For a visual inspection of reconstruction results, we provide

Fig. 8. Reconstructions of the FORBILD thorax phantom using DBP-0 (left) and WFBP (right). Top: slice $z = -0.8$ cm, Middle: slice $y = 0$, Bottom: slice $x = 0$. Window: $-25 \ldots 25$ HU.

reconstructions of the FORBILD thorax phantom from both methods in fig. 8. As one expects from an exact reconstruction algorithm, there are no cone-beam artifacts visible in the DBP-0 reconstruction result, whereas severe cone-beam artifacts can be observed in the WFBP reconstruction results.

V. Discussion and Conclusion

We have presented some extensions to the DBP-0 reconstruction method: a reconstruction method taking the desired slice thickness into account, ROI reconstruction, a way of incorporating flying focal spot data and a frequency apodization scheme. We have shown that using these extensions the DBP-0 method gains flexibility, making it more suitable for the use in clinical scanners. We also have shown images which were reconstructed from real data using DBP-0 and have compared DBP-0 reconstruction results to reconstructions obtained with WFBP, an approximate method currently used in clinical CT scanners. Our results show that WFBP features a slightly better resolution vs. noise level due to a better utilization of the detector data. However, this difference is qualified by the fact that DBP-0, in contrast to WFBP, does not show cone-beam artifacts in the reconstructed image.

References

[1] A. Katsevich, "Analysis of an exact inversion algorithm for spiral cone-beam CT," *Phys. Med. Biol.*, vol. 47, pp. 2583–2597, 2002.

[2] J. Pack, F. Noo, and R. Clackdoyle, "Cone-beam reconstruction using the backprojection of locally filtered projections," *IEEE Trans. Med. Imag.*, vol. 24, no. 1, pp. 70–85, Jan. 2005.

[3] N. Zuo, D. Xia, Y. Zou, T. Jiang, and X.-C. Pan, "Chord-based image reconstruction in cone-beam CT with a curved detector," *Med. Phys.*, vol. 33, no. 10, pp. 3743–3757, Oct. 2006.

[4] K. Stierstorfer, A. Rauscher, J. Boese, H. Bruder, S. Schaller, and T. Flohr, "Weighted FBP - a simple approximate 3D FBP algorithm for multislice spiral CT with good dose usage for arbitrary pitch," *Phys. Med. Biol.*, vol. 49, pp. 2209–2218, 2004.

[5] H. Schöndube, K. Stierstorfer, F. Dennerlein, T. White, and F. Noo, "Towards an efficient two-step hilbert algorithm for helical cone-beam CT," in *Proc. 2007 Meeting on Fully 3D Image Reconstruction in Radiology and Nuclear Medicine (Lindau, Germany)*, F. Beekman and M. Kachelrieß, Eds., 2007, pp. 120–123.

[6] H. Söhngen, "Die Lösungen der Integralgleichung $g(x) = \frac{1}{2\pi}\int_{-a}^{a}\frac{f(\xi)}{x-\xi}d\xi$ und deren Anwendung in der Tragflügeltheorie," *Math. Z.*, vol. 45, pp. 245–264, 1937.

[7] T. Flohr, K. Stierstorfer, H. Bruder, J. Simon, A. Polacin, and S. Schaller, "Image reconstruction and image quality evaluation for a 16-slice CT scanner," *Med. Phys.*, vol. 30, no. 5, pp. 832–845, May 2003.